Chemical Science

ROYAL SOCIETY OF CHEMISTRY

EDGE ARTICLE

View Article Online
View Journal | View Issue

Cite this: *Chem. Sci.*, 2023, **14**, 8823

All publication charges for this article have been paid for by the Royal Society of Chemistry

Received 13th July 2023
Accepted 29th July 2023

DOI: 10.1039/d3sc03593j

rsc.li/chemical-science

Ligand-protected nanocluster-mediated photoswitchable fluorescent nanoprobes towards dual-color cellular imaging†

Wencheng Zhong,[a] Kangqiang Liang,[a] Wenfeng Liu[a] and Li Shang *[abc]

Development of robust multi-color photoswitchable fluorescent probes is critical for many optical applications, but it remains a challenge to rationally design these probes. Here, we report a new design of Förster resonance energy transfer-based dual-color photoswitchable fluorescent nanoparticles (DPF NPs) by taking advantage of the distinct properties of ligand-protected gold nanoclusters (AuNCs). Detailed photophysical studies revealed that ultrasmall-sized AuNCs not only act as the FRET donors due to their intrinsic fluorescence properties, but also play a significant role in regulating the photochromic and aggregate properties of spiropyran through ligand–spiropyran interactions. These DPF NPs exhibit a high fluorescence on/off ratio (~90%) for both green and red fluorescence emission, and good reversibility during cycled photo-stimulation. Cell imaging experiments showed that DPF NPs could specifically accumulate in lipid droplets, and enable photoswitchable dual-color imaging in living cells. Moreover, by labeling mitochondria with a green-emitting marker, we demonstrated that DPF NPs can distinguish different targets based on dynamic and static fluorescence signals at the sub-cellular level in two emission channels reliably. This study provides a new strategy for designing robust photoswitchable fluorescent probes by modulating the properties of photochromic dyes through ligand-protected nanoclusters, which can be generalized for the development of other photoswitch systems towards advanced optical applications.

Introduction

Photocontrolled fluorescence switches have been widely used in many fields, such as anti-counterfeiting,[1] smart materials,[2] enzyme engineering,[3] gate-controlled delivery[4] and optical imaging.[5] Typically, photocontrolled fluorescence switches can be divided into a single-color fluorescence switch and multi-color fluorescence switch.[6–8] Compared with the mostly studied single-color photoswitch system, the latter can provide multi-dimensional information per time, and thus is more attractive for advanced optical applications.[9–11] For example, Yu *et al.*[12] designed a class of photoswitchable tristate fluorescent polymeric nanoparticles, which exhibit high contrast and excellent photoreversibility that favor advanced optical anti-counterfeiting. Recently, Yang *et al.*[13] reported a novel triple fluorescence switching through multiphoton manipulation, which showed great potential in dual-color super-resolution cellular imaging.

As the key module of a photocontrolled fluorescence switch, the properties of photochromic dyes play essential roles in determining the performance of the system.[14–18] In particular, recent studies revealed that the feature of the local microenvironment of photochromic dyes, *e.g.*, hydrophobicity and spatial flexibility, can strongly affect their photochromism properties.[19–21] While local hydrophobicity is favorable for the dyes to retain their photochromic properties, spatial flexibility can provide the necessary space for the isomerization process. Consequently, to enhance the performance of the photoswitch system (*e.g.*, on/off ratio, fatigue resistance and switch rate), researchers have proposed different strategies to regulate the properties of photochromic dyes, such as encapsulation in polymers[22,23] and biomolecules.[24,25] Nevertheless, these strategies often require a complicated synthesis process, and the performance of the fabricated fluorescence photoswitch is still limited. Apparently, effectively regulating the microenvironment around photochromic dyes *via* a simple strategy is important for advancing the application of a fluorescence photoswitch, which has remained challenging up to now.

Recently, fluorescent inorganic nanoparticles (NPs) have shown great potential in constructing a photocontrolled fluorescence switch owing to their excellent photophysical

[a]State Key Laboratory of Solidification Processing, School of Materials Science and Engineering, Northwestern Polytechnical University (NPU), Xi'an 710072, China. E-mail: li.shang@nwpu.edu.cn

[b]Research & Development Institute of Northwestern Polytechnical University in Shenzhen, Shenzhen 518057, China

[c]Chongqing Science and Technology Innovation Center of Northwestern Polytechnical University, Chongqing 401135, China

† Electronic supplementary information (ESI) available. See DOI: https://doi.org/10.1039/d3sc03593j

properties, good biocompatibility and controllable synthesis.[26–30] In particular, surface ligand layers of inorganic NPs can act as effective mediators to regulate the interactions between the inorganic core and photochromic dyes, which make them attractive in modulating the microenvironment of photochromic dyes on the surface of these NPs. So far, a variety of nanoparticles have been used to construct photocontrolled fluorescence switches, such as semiconductor quantum dots,[31] upconverting NPs,[32] perovskite nanocrystals[33] and metal nanoclusters.[34] However, multi-color fluorescence photoswitches based on ligand-protected NPs have rarely been achieved,[34–36] and the distinct capability of NPs for modulating the photophysical properties of photochromic dyes has not been adequately exploited.[6,37,38] Photoisomerization kinetics of photochromic compounds is regarded as an important issue in determining their performance in applications.[16,39] Thus, a deep understanding of photoisomerization kinetics is essential for precisely controlling their photochromic properties, which was largely missing in many previous studies.[34–38] In particular, the underlying rationale for regulating their photoswitching performance (*e.g.* on/off ratio and anti-fatigue property) still needs further clarification.

Herein, we report the design of dual-color photoswitchable fluorescent NPs (DPF NPs) by the assembly of green-emitting gold nanoclusters (AuNCs) and photochromic spiropyran with red fluorescence. AuNCs were chosen as the model fluorescent NPs mainly due to their ultrasmall size, good biocompatibility and well-defined structures.[40–44] Compared to organic dyes, the large specific surface area and the easily tunable surface properties of AuNCs are beneficial for regulating the photochromic properties of photochromic dyes. Based on the efficient fluorescence resonance energy transfer (FRET) between AuNCs and spiropyran, both green and red fluorescence of the fabricated DPF NPs can be reversibly switched on/off upon a light stimulus (Scheme 1A). Interestingly, besides acting as the FRET donor, AuNCs were also found to actively regulate the photochromic properties of spiropyran within the NPs. Surface ligands of AuNCs (arginine and 6-aza-2-thiothymine, Arg/ATT) can not only induce deprotonation of the protonated merocyanine (MCH^+) state, but also regulate the aggregate behavior of the merocyanine (MC) state on the surface of AuNCs. The fabricated DPF NPs possess excellent fatigue resistance and a high on/off ratio (~90%) for both green and red fluorescence emission, making them promising nanoprobes for multi-color bioimaging applications. As an example, we demonstrate the potential use of these DPF NPs for effectively differentiating static and dynamic fluorescence signals from different sub-cellular compartments (Scheme 1B).

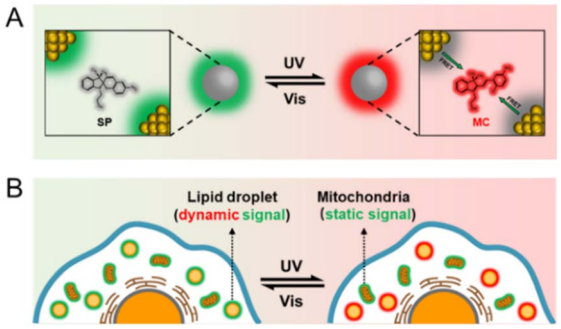

Scheme 1 (A) Schematic diagram of the design principle of DPF NPs, and (B) illustration of differentiating static and dynamic fluorescence signals from different sub-cellular compartments by employing DPF NPs as probes.

Results and discussion

Photochromic spiropyran can reversely transform from the non-fluorescent SP state into the MC state with red emission under the irradiation of UV light (Fig. S1†), and acts as the FRET acceptor in the present fluorescence switch. As reported by Deng *et al.*, Arg-modified ATT-AuNCs (Arg/ATT-AuNCs) exhibit a high quantum yield.[45] The absolute quantum yield of as-prepared AuNCs was measured to be 46.5 ± 0.5% (Fig. S2†). The size of green emitting Arg/ATT-AuNCs was measured to be 2.0 ± 0.2 nm from transmission electron microscopy (TEM) analysis (Fig. S3†). The ultrasmall size of AuNCs is also expected to increase the surface area in contact with spiropyran. Therefore, ultrasmall AuNCs with high quantum yield were chosen as the FRET donor to construct a FRET pair. As seen in Fig. 1A, the UV-vis absorption spectrum of MC showed a strong absorption peak at 540 nm in the visible region, while Arg/ATT-AuNCs exhibited a narrow fluorescence band with the maximum at 530 nm. The significant overlap between the emission spectrum of AuNCs and the absorption spectrum of spiropyran provides an important prerequisite for switching the fluorescence of

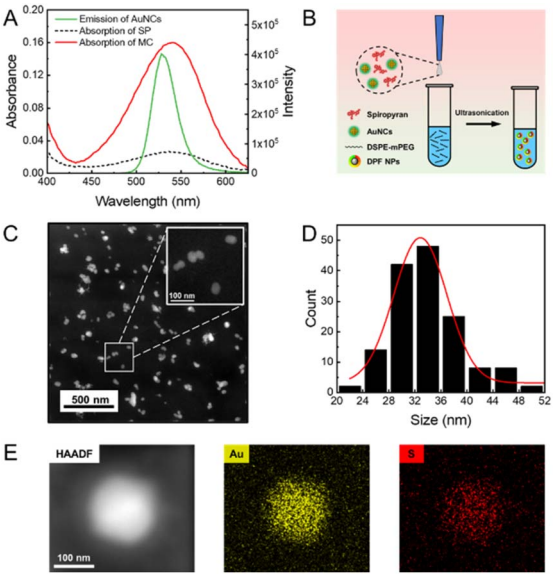

Fig. 1 (A) Fluorescence emission spectra of AuNCs in aqueous solution (excitation wavelength: 405 nm) and absorption spectra of SP/MC in ethanol. (B) Scheme of the preparation of DPF NPs. (C) Representative TEM image of DPF NPs in high-angle annular dark-field (HADDF) mode. The inset photograph is the enlarged version of several DPF NPs. (D) Size distribution histogram of DPF NPs based on TEM images. (E) EDS element mapping of Au and S in an individual DPF NP.

AuNCs *via* FRET. Under the state of MC or SP, the overlapping degree is remarkably different, allowing us to further control the FRET efficiency *via* a UV/vis light stimulus. To ensure that the distance between AuNCs and spiropyran meets the FRET requirement (<10 nm), the lipid-mediated nanoprecipitation method was adopted to encapsulate both components (Fig. 1B).[46] In particular, 1,2-distearoyl-*sn*-glycero-3-phosphoethanolamine with conjugated methoxyl poly(ethylene glycol) (DSPE-mPEG) was selected as the self-assembling reagent to form NPs with reasonable aqueous solubility.[47,48] The transmission electron microscopy (TEM) images showed that the resulting DPF NPs are well-dispersed with an average diameter of 35 ± 7 nm (Fig. 1C and D). Their hydrodynamic size was determined to be 52 ± 4 nm by dynamic light scattering measurement (Fig. S4†), which is larger than that measured by TEM due to the extra hydration layers from the outside components.[49] The energy dispersive spectroscopy (EDS) results further showed a uniform distribution of Au and S elements (Fig. 1E), indicating the successful encapsulation of AuNCs in lipid-coated NPs.

As a photochromic dye with intrinsic fluorescence, spiropyran exhibits weak fluorescence in the SP state, but becomes highly fluorescent with the emission peak at 650 nm in the MC state upon the UV stimulus (Fig. S5†). As seen in the inset photograph of Fig. 2A, as-prepared DPF NPs exhibit green fluorescence from AuNCs when spiropyran is in the SP state. Upon irradiation by UV light at 365 nm, the solution gradually became red fluorescent originating from the MC state of spiropyran as expected.[50,51] Meanwhile, the green fluorescence of AuNCs was effectively inhibited due to the energy transfer from AuNCs to the MC state of spiropyran. Indeed, the fluorescence spectra of DPF NPs exhibited significant changes upon UV light irradiation, as shown in Fig. 2A. The intensity of green fluorescence decreased accompanied by a gradual increase in red fluorescence, indicating the occurrence of an effective FRET process (Fig. 2B). Fluorescence decay of AuNCs before and after illumination with UV light was also measured. As seen in Fig. S6 and Table S1,† the average fluorescence lifetime of AuNCs decreased from 10.77 ± 0.14 ns to 2.72 ± 0.04 ns after UV light illumination, further confirming the occurrence of FRET between AuNCs and spiropyran. In addition, the Förster distance (R_0) was measured to be 6.4 nm, and the FRET efficiency was calculated to be 90% (see details in the ESI†). Note that although the size of DPF NPs is beyond the distance for FRET to occur, the high local molecular density and confinement effect within the lipid NPs still ensure effective FRET between AuNCs and spiropyran.[52] Moreover, the ratio of SP to AuNCs in DPF NPs affects the FRET efficiency, and a lower ratio will lead to a decreased efficiency (Fig. S7†). Compared to monomer MC, the fluorescence peak of MC in DPF NPs shows a slight blue shift from 650 nm to 645 nm, suggesting that the microenvironment of spiropyran is changed upon encapsulation inside lipid NPs.

The switching reversibility of these DPF NPs was then evaluated upon irradiating the solution with UV and visible light alternatively. As shown in Fig. 2C, both green and red emission of DPF NPs could be reversibly switched on/off for at least 10 cycles. Although the intensity signal showed slight fatigue during the cycled irradiation, the fluctuation of the switching ratio for either green emission or red emission was calculated to be less than 5%, indicating a good stability of DPF NP-based photoswitches (Fig. 2D). Further quantitative analysis revealed that the on/off ratio of the present photoswitch system is up to 90% for both green and red emission colors (Fig. S8†). We note that such a high multicolor switching ratio has been rarely achieved in the reported multi-color fluorescence photoswitchable nanoprobes.[36,53–56] Previous studies found that fluorescent switches fabricated by noncovalently conjugating the fluorescence donor with the photochromic acceptor are more favorable for achieving a high switching ratio than that constructed by covalent binding.[57–60] Thus, instead of covalent conjugation, we adopted a rather mild strategy by physically encapsulating both AuNCs and spiropyran inside lipid NPs. Meanwhile, the noncovalent method also minimizes potential influence towards the photophysical properties of AuNCs and spiropyran, which may also contribute to the high switching ratio of the present system.

One big challenge for the biological application of a spiropyran-based photoswitch is its poor stability in an aqueous medium.[61,62] In particular, interactions between spiropyran and ligand-protected NPs can strongly affect its photochromic behavior in a biological environment, which consequently determines the performance of the fluorescent photoswitch system. Therefore, to elucidate the underlying switching mechanism of the present system, we then investigated the effect of the surface ligands of AuNCs on the properties of spiropyran. Since Arg is located in the outer layer of AuNCs, we assume that these Arg molecules may play a key role in mediating their interactions with spiropyran. As seen in Fig. 3A, there is a shoulder peak at 430 nm in the absorption spectra of spiropyran dispersed in DSPE-mPEG, which is known as the characteristic peak of protonated MC (MCH^+).[63] However, in the

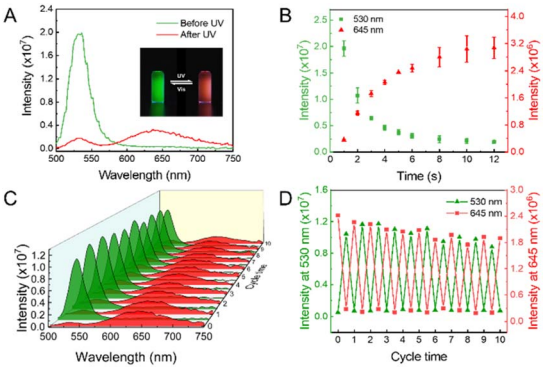

Fig. 2 (A) Fluorescence emission spectra of DPF NPs before and after UV irradiation. Excitation wavelength: 405 nm (inset photograph: photocontrolled dual-color fluorescence switching of DPF NPs in aqueous solution). (B) Time-dependent fluorescence intensity change of DPF NPs at 530 nm and 645 nm under UV irradiation. (C) Fluorescence spectra of DPF NPs during several 365 nm/520 nm light irradiation cycles. Excitation wavelength: 405 nm. (D) Change of fluorescence intensity at 530 nm and 645 nm upon cycled irradiation 10 times.

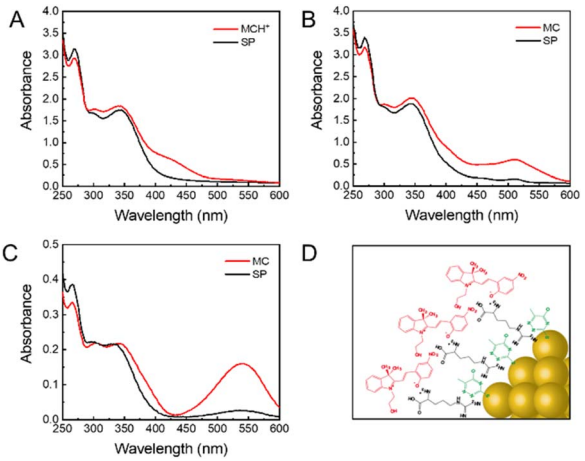

Fig. 3 Absorption spectra of (A) SP@DSPE-mPEG, (B) DPF NPs in aqueous solution, and (C) SP/MC in ethanol. (D) Scheme of the proposed arrangement of MC on the surface of Arg/ATT-AuNCs.

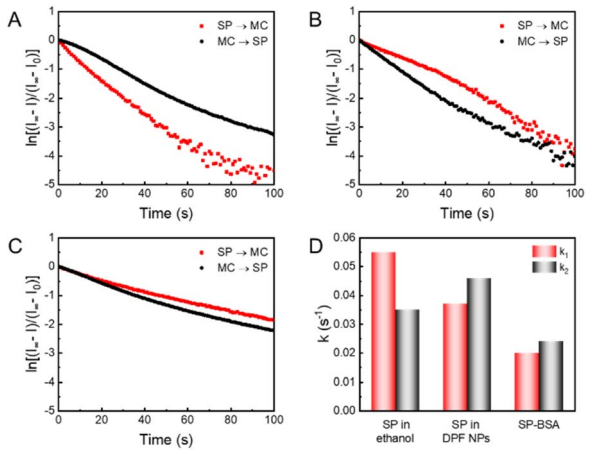

Fig. 4 Photochromic kinetics of (A) spiropyran in ethanol, (B) spiropyran in DPF NPs and (C) SP-BSA in aqueous solution during the coloring and discoloring process. (D) Comparison of rate constants of SP → MC (k_1) and MC → SP (k_2) based on data in A–C.

presence of Arg/ATT-AuNCs, the shoulder peak at 430 nm moved to 512 nm that corresponds to the MC state of spiropyran (Fig. 3B). As a control, we also measured the spectral change of AuNCs without Arg layers (ATT-AuNCs) in DSPE-mPEG. In stark contrast, the absorption spectra of ATT-AuNCs did not show a similar change to that of Arg/ATT-AuNCs (Fig. S9†). Consistent with the absorption spectral change, a similar phenomenon was also observed in the excitation spectra. As seen in Fig. S10,† compared with MCH^+ in DSPE-mPEG, the characteristic excitation band of MC at 550 nm increased significantly in the excitation spectrum of DPF NPs.

Altogether, these observations suggest that Arg on the surface of AuNCs is likely the main reason for the red shift in the absorption spectra. Previous studies showed that the MC state usually exhibits a stronger affinity with zwitterionic Arg than the SP state.[64] As illustrated in Fig. S11,† deprotonation of MCH^+ would happen when it comes into contact with Arg on the surface of AuNCs, leading to the transformation from MCH^+ into MC. Therefore, the deprotonation process of MCH^+ induced by Arg is indispensable for FRET between AuNCs and spiropyran. Moreover, the aggregate behavior of MC was also affected by the surface ligands of AuNCs. As seen in Fig. 3C, free MC possesses an adsorption peak at 540 nm in ethanol. In contrast, MC in DPF NPs shows a blue-shifted peak at 510 nm, which implies that MC may form H-aggregates in DFP NPs upon interacting with the surface of AuNCs.[65,66] As illustrated in Fig. 3D, the oriented interactions between Arg on AuNCs and MC lead to an ordered arrangement of MC in the form of head-to-head aggregates. Apparently, in the present photoswitching system, the surface ligands of AuNCs play an essential role in effectively mediating the microenvironment and aggregate behaviors of photochromic spiropyran.

To further understand the interactions between spiropyran and the surface of AuNCs, photochromic kinetics of spiropyran in DPF NPs were investigated by monitoring the fluorescence of MC. As shown in Fig. 4A, spiropyran exhibited different photochromic rates in ethanol under irradiation with UV and vis light, which corresponds to the coloring (SP → MC) and discoloring (MC → SP) process, respectively. Further quantitative analysis revealed that the rate constant k_1 of the SP → MC process (0.055 s^{-1}) was higher than the rate constant k_2 of the MC → SP process (0.035 s^{-1}), indicating that the reaction SP → MC is more preferred in ethanol. However, for spiropyran in DPF NPs, the photochromic rate k_1 (0.037 s^{-1}) became lower than k_2 (0.046 s^{-1}), suggesting that the photochromic kinetics of spiropyran was reversed in DPF NPs (Fig. 4B). Moreover, the photochromic kinetic curve of SP in DFP NPs deviated slightly from the curve of the first-order kinetics, indicating that the aggregation of MC agrees well with the results of the absorption spectra.[67] We hypothesize that noncovalent interactions between spiropyran and AuNCs in DPF NPs can still provide sufficient steric flexibility for the photoisomerization of spiropyran. To test the above hypothesis, the photochromic kinetics of SP covalently attached to bovine serum albumin (SP-BSA) was studied. Indeed, the photoisomeric degree of spiropyran in SP-BSA was significantly affected, which led to a slowdown of the SP/MC photochromism, as shown in Fig. 4C. Compared to the photochromic rates of SP in DPF NPs and ethanol, both k_1 and k_2 were decreased significantly in SP-BSA (Fig. 4D). It can be concluded that the steric flexibility for the photochromism of SP/MC is still well retained despite its interaction with the surface of AuNCs, which then contributes to the high on/off ratio of the DPF NP-based fluorescence switch.

A photocontrolled fluorescence switch with a reversible and high on/off ratio could provide a fluorescence signal with enhanced contrast, and holds great potential as robust optical probes for high-resolution bioimaging. To evaluate the potential use of the present DPF NPs for cell imaging, CCK-8 assay was first performed to evaluate their cytocompatibility. Fig. S12† shows that there was no obvious decrease in cell viability in the presence of up to 100 μM (the concentration of Au) DPF NPs, indicating a low cytotoxicity. Moreover, control

studies have been performed to ensure negligible phototoxicity under the experimental conditions (Fig. S13†). As shown in Fig. 5A, the fluorescence signal in both green and red channels was captured at different times after incubating DPF NPs with HeLa cells. Herein, only a strong fluorescence signal in the green channel was observed in the beginning, and there was no fluorescence in the red channel as expected. Under continuous exposure to 405 nm light, the fluorescence signal in the green channel decreased gradually with a synchronous increase in red emission (Fig. 5B). This is more evident from the overlay images, where the pseudo color of fluorescence images in HeLa cells turned from green to yellow, and finally to red. This phenomenon indicates the occurrence of FRET between AuNCs and MC in DPF NPs in the cellular environment, which is in good agreement with the above results in the solution. In addition, the Pearson colocalization coefficient of the green and red channels was calculated to be 0.89, which indicates that DPF NPs retain good structural integrity inside living cells (Fig. S14†). Interestingly, these DPF NPs were found to specifically localize in the lipid droplets, as confirmed by using a commercial lipid droplet marker, BODIPY 493/503.[68] As shown in Fig. S15,† Pearson's colocalization coefficient of BODIPY 493/503 and DPF NPs is 0.83, suggesting a remarkable accumulation of DPF NPs in cellular lipid droplets, which is likely derived from the amphiphilicity of DSPE-mPEG.[69] As shown in Fig. 5C, green fluorescence in lipid droplets will gradually turn to red fluorescence under irradiation with UV light. Subsequently, red fluorescence in lipid droplets will recover to green fluorescence under irradiation with visible light. The reversible signal change showed that DPF NPs still retain the property of reversible fluorescence photoswitching in a living cellular environment. Further quantitative analysis as shown in Fig. 5D showed that DPF NPs possessed good photostability during the multi-cycled photoswitching process, suggesting the great potential of DPF NPs as robust probes for advanced cell imaging applications, such as super-resolution imaging[70] and long-term tracking.[71]

Compared with a single-color fluorescence switch, a dual-color fluorescence switch can provide a more reliable and precise imaging capability. In particular, a reversible dual-color fluorescence photoswitch enables different targets to be distinguished based on dynamic and static fluorescence signals. As an example, we further evaluated the capability of DPF NPs to distinguish fluorescence signals in lipid droplets from mitochondria that were stained using MitoTracker™ Green in HeLa cells. As shown in Fig. 6A, before activating the photoswitching properties of DPF NPs, it is hard to distinguish the location of lipid droplets from mitochondria because both organelles emit fluorescence in the green channel. However, under continuous irradiation with UV light for 5 seconds (405

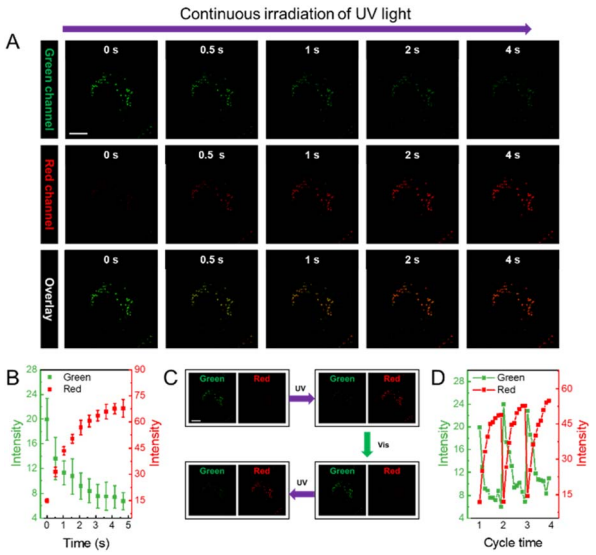

Fig. 5 (A) Time-dependent fluorescence images of DPF NP-incubated HeLa cells under UV irradiation in different emission channels (scale bar: 10 μm). (B) Fluorescence intensity changes of green and red channels *versus* the irradiation time based on fluorescence images. (C) Dual-fluorescence signal change in HeLa cells upon cycled irradiation with UV/vis light (scale bar: 10 μm). (D) Changes in the fluorescence intensity of green and red channel upon cycled irradiation with UV/vis light.

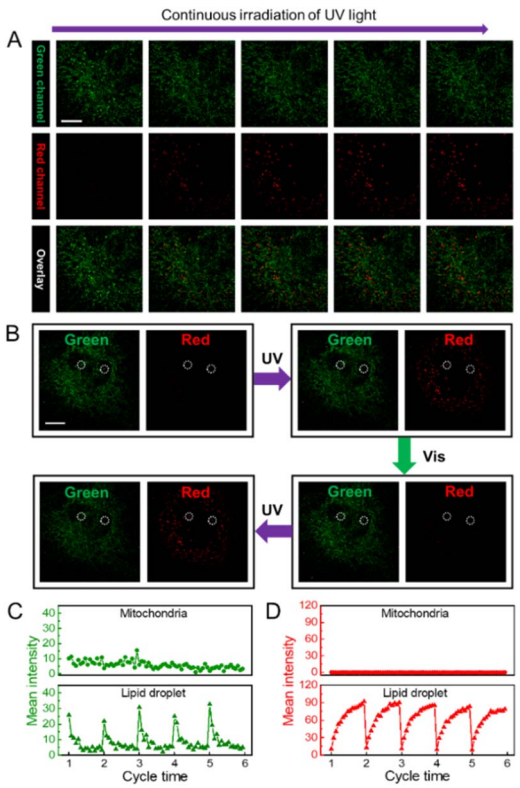

Fig. 6 (A) Time-dependent fluorescence images of HeLa cells upon labelling with DPF NPs and MitoTracker™ Green under UV irradiation in different emission channels (scale bar: 10 μm). (B) Fluorescence images of HeLa cells upon labelling with DPF NPs and MitoTracker™ Green under cycled irradiation with UV/vis light in green and red channels. White circles in the images indicate two representative lipid droplets identified based on the dynamic signals. Changes in the fluorescence intensity of the (C) green channel and (D) red channel in mitochondria (upper) and lipid droplets (lower) of HeLa cells upon cycled irradiation with UV/vis light.

nm), the fluorescence signal in the green channel will partly decrease accompanied by a significant increase in fluorescence in the red channel due to the activation of DPF NPs. Upon further irradiation with visible light (552 nm), fluorescence signals in both green and red channels will recover back due to the reversible photoswitching properties of DPF NPs (Fig. 6B). It is noteworthy that the fluorescence signal of mitochondria that were stained using non-photoswitchable fluorophores will only be randomly fluctuating, mostly in a "static mode" (Fig. S16†). In stark contrast, fluorescence signals from DPF NP-labelled lipid droplets will exhibit reversible switching on/off states, in a "dynamic mode". In this way, fluorescence signals from two different cell organelles can be easily distinguished based on the dynamic and static nature of the labelling probes. Indeed, quantitative analysis in Fig. 6C showed that during the cycled UV/vis light irradiation, fluorescence signals in MitoTracker™ Green-stained mitochondria remained essentially unaltered in the green channel. However, for DPF NP-stained lipid droplets, fluorescence signals in the green channel displayed a cycled turn on/off feature, allowing both signals to be easily distinguished. Moreover, thanks to the dual-color fluorescence properties of DPF NPs, one can also distinguish two organelles in the red emission channel. As seen in Fig. 6D, similar to that in the green channel, highly dynamic and switchable fluorescence signals could be observed for DPF NP-stained lipid droplets in the red channel, while the emission of mitochondria was always in the dark state. Therefore, a more reliable targeted imaging of cell organelles can be easily achieved by using these dual-color photoswitchable NPs, which also enrich the toolbox of available dyes for bioimaging application.

Conclusions

In summary, we have developed a new strategy for synthesizing fluorescence photoswitchable nanoprobes by modulating the microenvironment of photochromic dyes based on the distinct roles of ligand-protected NPs. With Arg/ATT-AuNCs as an example, we demonstrated the fabrication of dual-color photoswitchable fluorescent NPs with a high on/off ratio (~90%) for both green and red emission. In particular, AuNCs can effectively regulate the photochromic and aggregate properties of spiropyran through their surface ligands, which is essential for the good photoswitching performance of the resulting NPs. The distinct fluorescence switching properties of these DPF NPs can be used to effectively distinguish dynamic and static fluorescence signals in different sub-cellular compartments (*e.g.* lipid droplets and mitochondria), which make them promising nanoprobes for versatile fluorescence imaging applications, such as super-resolution imaging and multi-target tracking. Moreover, this work also provides a new, generable strategy for developing advanced photocontrolled fluorescence switches based on various ligand-protected NPs.

Data availability

Data are available on request to the authors.

Author contributions

W. Z. conceived the project, performed the experiment and wrote the draft. K. L. assisted with the experiments and data analysis. W. L. assisted with the experiments. L. S. supervised the project, assisted with the data analysis and finalized the manuscript.

Conflicts of interest

The authors declare no conflict of interest.

Acknowledgements

This work was supported by the National Natural Science Foundation of China (22274131), the Shenzhen Science and Technology Program (Grant No. JCYJ20220530161800001), the Natural Science Foundation of Chongqing (cstc2021jcyj-msxmX0980), the Innovation Foundation for Doctor Dissertation of Northwestern Polytechnical University (CX2021053) and the Research Fund of the State Key Laboratory of Solidification Processing (NPU, 2020-QZ-01).

Notes and references

1 Y. Liu, S. Liang, C. Yuan, A. Best, M. Kappl, K. Koynov, H. J. Butt and S. Wu, *Adv. Funct. Mater.*, 2021, **31**, 2103908.
2 K. Imato, K. Momota, N. Kaneda, I. Imae and Y. Ooyama, *Chem. Mater.*, 2022, **34**, 8289–8296.
3 J. Chai, Y. Zhao, L. Xu, Q. Li, X. Y. Hu, D. S. Guo and Y. Liu, *Angew. Chem., Int. Ed.*, 2022, **61**, e202116073.
4 Y. Kim, R. Thangam, J. Yoo, J. Heo, J. Y. Park, N. Kang, S. Lee, J. Yoon, K. R. Mun, M. Kang, S. Min, S. Y. Kim, S. Son, J. Kim, H. Hong, G. Bae, K. Kim, S. Lee, L. Yang, J. Y. Lee, J. Kim, S. Park, D. H. Kim, K. B. Lee, W. Y. Jang, B. H. Kim, R. Paulmurugan, S. W. Cho, H. C. Song, S. J. Kang, W. Sun, Y. Zhu, J. Lee, H. J. Kim, H. S. Jang, J. S. Kim, A. Khademhosseini, Y. Kim, S. Kim and H. Kang, *Adv. Mater.*, 2022, **34**, 2205498.
5 D. Kim, A. Aktalay, N. Jensen, K. Uno, M. L. Bossi, V. N. Belov and S. W. Hell, *J. Am. Chem. Soc.*, 2022, **144**, 14235–14247.
6 D. Kim and S. Y. Park, *Adv. Opt. Mater.*, 2018, **6**, 1800678.
7 M. Olesinska-Monch and C. Deo, *Chem. Commun.*, 2023, **59**, 660–669.
8 W. Zhang, F. Huo, Y. Yue, Y. Zhang, J. Chao, F. Cheng and C. Yin, *J. Am. Chem. Soc.*, 2020, **142**, 3262–3268.
9 Q. Qi, C. Li, X. Liu, S. Jiang, Z. Xu, R. Lee, M. Zhu, B. Xu and W. Tian, *J. Am. Chem. Soc.*, 2017, **139**, 16036–16039.
10 G. Naren, C. W. Hsu, S. Li, M. Morimoto, S. Tang, J. Hernando, G. Guirado, M. Irie, F. M. Raymo, H. Sunden and J. Andreasson, *Nat. Commun.*, 2019, **10**, 3996.
11 Y. H. Chan, M. E. Gallina, X. J. Zhang, I. C. Wu, Y. H. Jin, W. Sun and D. T. Chiu, *Anal. Chem.*, 2012, **84**, 9431–9438.
12 M. Yu, P. Zhang, L. Liu, H. Wang, H. Wang, C. Zhang, Y. Gao, C. Yang, J. Cui and J. Chen, *Adv. Opt. Mater.*, 2021, **9**, 2101227.

13 R. Yang, X. Ren, L. Mei, G. Pan, X. Z. Li, Z. Wu, S. Zhang, W. Ma, W. Yu, H. H. Fang, C. Li, M. Q. Zhu, Z. Hu, T. Sun, B. Xu and W. Tian, *Angew. Chem., Int. Ed.*, 2022, **61**, e202117158.
14 C. R. Martin, K. C. Park, G. A. Leith, J. Yu, A. Mathur, G. R. Wilson, G. B. Gange, E. L. Barth, R. T. Ly, O. M. Manley, K. L. Forrester, S. G. Karakalos, M. D. Smith, T. M. Makris, A. K. Vannucci, D. V. Peryshkov and N. B. Shustova, *J. Am. Chem. Soc.*, 2022, **144**, 4457–4468.
15 E. Chatir, A. Khettabi, F. Lafolet, D. Jouvenot, G. Royal, E. Saint-Aman and S. Cobo, *Chem. Mater.*, 2022, **34**, 5912–5918.
16 A. Meeks, M. M. Lerch, T. B. H. Schroeder, A. Shastri and J. Aizenberg, *J. Am. Chem. Soc.*, 2022, **144**, 219–227.
17 K. Mutoh, N. Miyashita, K. Arai and J. Abe, *J. Am. Chem. Soc.*, 2019, **141**, 5650–5654.
18 Y. Xiong, P. Rivera-Fuentes, E. Sezgin, A. Vargas Jentzsch, C. Eggeling and H. L. Anderson, *Org. Lett.*, 2016, **18**, 3666–3669.
19 A. B. Grommet, L. M. Lee and R. Klajn, *Acc. Chem. Res.*, 2020, **53**, 2600–2610.
20 S. Osella and S. Knippenberg, *J. Am. Chem. Soc.*, 2017, **139**, 4418–4428.
21 P. Q. Nhien, T. T. K. Cuc, T. M. Khang, C. H. Wu, B. T. B. Hue, J. I. Wu, B. W. Mansel, H. L. Chen and H. C. Lin, *ACS Appl. Mater. Interfaces*, 2020, **12**, 47921–47938.
22 J. Chen, F. Zeng, S. Z. Wu, J. Su and Z. Tong, *Small*, 2009, **5**, 970–978.
23 M. Tao, X. Liang, J. Guo, S. Zheng, Q. Qi, Z. Cao, Y. Mi and Z. Zhao, *ACS Appl. Mater. Interfaces*, 2021, **13**, 33574–33583.
24 X. Chai, H. H. Han, A. C. Sedgwick, N. Li, Y. Zang, T. D. James, J. Zhang, X. L. Hu, Y. Yu, Y. Li, Y. Wang, J. Li, X. P. He and H. Tian, *J. Am. Chem. Soc.*, 2020, **142**, 18005–18013.
25 J. Zhang, Y. Fu, H. H. Han, Y. Zang, J. Li, X. P. He, B. L. Feringa and H. Tian, *Nat. Commun.*, 2017, **8**, 987.
26 L. Shang and G. U. Nienhaus, *Mater. Today*, 2013, **16**, 58–66.
27 Y. Zhang, K. Zhang, J. Wang, Z. Tian and A. D. Li, *Nanoscale*, 2015, **7**, 19342–19357.
28 K. Zheng, S. Han, X. Zeng, Y. Wu, S. Song, H. Zhang and X. Liu, *Adv. Mater.*, 2018, **30**, e1801726.
29 H. Wu, Y. Chen, X. Dai, P. Li, J. F. Stoddart and Y. Liu, *J. Am. Chem. Soc.*, 2019, **141**, 6583–6591.
30 Y. Akaishi, A. D. Pramata, S. Tominaga, S. Kawashima, T. Fukaminato and T. Kida, *Chem. Commun.*, 2019, **55**, 8060–8063.
31 S. Padgaonkar, C. T. Eckdahl, J. K. Sowa, R. López-Arteaga, D. E. Westmoreland, E. F. Woods, S. Irgen-Gioro, B. Nagasing, T. Seideman, M. C. Hersam, J. A. Kalow and E. A. Weiss, *Nano Lett.*, 2021, **21**, 854–860.
32 C. Liu, X. Zheng, T. Dai, H. Wang, X. Chen, B. Chen, T. Sun, F. Wang, S. Chu and J. Rao, *Angew. Chem., Int. Ed.*, 2022, **61**, e202116802.
33 Y. Akaishi, A. Mokhtar, M. Shimoyoshi, T. Nohara, Y. Inomata, D. Kosumi, T. Fukaminato and T. Kida, *Small*, 2022, **18**, 2205046.
34 Y. Cong, X. Wang, S. Zhu, L. Liu and L. Li, *ACS Appl. Bio Mater.*, 2021, **4**, 2790–2797.
35 I. L. Medintz, S. A. Trammell, H. Mattoussi and J. M. Mauro, *J. Am. Chem. Soc.*, 2004, **126**, 30–31.
36 M. F. Budyka, P. A. Nikulin, T. N. Gavrishova and O. V. Chashchikhin, *ChemPhotoChem*, 2021, **5**, 582–590.
37 S. A. Diaz, L. Giordano, T. M. Jovin and E. A. Jares-Erijman, *Nano Lett.*, 2012, **12**, 3537–3544.
38 D. Kim, K. Jeong, J. E. Kwon, H. Park, S. Lee, S. Kim and S. Y. Park, *Nat. Commun.*, 2019, **10**, 3089.
39 J. Wang, L. Avram, Y. Diskin-Posner, M. J. Białek, W. Stawski, M. Feller and R. Klajn, *J. Am. Chem. Soc.*, 2022, **144**, 21244.
40 L. Shang, J. Xu and G. U. Nienhaus, *Nano Today*, 2019, **28**, 100767.
41 T. Chen, H. Lin, Y. Cao, Q. Yao and J. Xie, *Adv. Mater.*, 2021, **34**, e2103918.
42 R. Jin, C. Zeng, M. Zhou and Y. Chen, *Chem. Rev.*, 2016, **116**, 10346–10413.
43 L. Zhang and E. Wang, *Nano Today*, 2014, **9**, 132–157.
44 W. Zhong, X. Yan, S. Qu and L. Shang, *Aggregate*, 2022, **4**, e245.
45 H.-H. Deng, X.-Q. Shi, F.-F. Wang, H.-P. Peng, A.-L. Liu, X.-H. Xia and W. Chen, *Chem. Mater.*, 2017, **29**, 1362–1369.
46 D. Song, M. Zhu, C. Li, Y. Zhou, Y. Xie, Z. Li and Z. Liu, *Anal. Chem.*, 2021, **93**, 16932–16939.
47 J. Li, Z. Zhang, X. Deng, Z. Xu, L. Wang, G. Xu, K. Wang, D. Wang and B. Z. Tang, *Biomaterials*, 2022, **287**, 121612.
48 K. Ma, S. Xu, T. Tao, J. Qian, Q. Cui, S. U. Rehman, X. Zhu, R. Chen, H. Zhao, C. Wang, Z. Qi, H. Dai, X. Zhang, C. Xie, Y. Lu, H. Wang and J. Wang, *Proc. Natl. Acad. Sci. U.S.A.*, 2022, **119**, e2211228119.
49 L. Shang, P. Gao, H. Wang, R. Popescu, D. Gerthsen and G. U. Nienhaus, *Chem. Sci.*, 2017, **8**, 2396–2400.
50 Y. Xue, J. Tian, W. Tian, P. Gong, J. Dai and X. Wang, *J. Phys. Chem. C*, 2015, **119**, 20762–20772.
51 M. Mandal, D. Banik, A. Karak, S. K. Manna and A. K. Mahapatra, *ACS Omega*, 2022, **7**, 36988–37007.
52 Y. Liu, G. Yang, S. Jin, R. Zhang, P. Chen, Tengjisi, L. Wang, D. Chen, D. A. Weitz and C. X. Zhao, *Angew. Chem., Int. Ed.*, 2020, **132**, 20240–20249.
53 S. A. Diaz, L. Giordano, J. C. Azcarate, T. M. Jovin and E. A. Jares-Erijman, *J. Am. Chem. Soc.*, 2013, **135**, 3208–3217.
54 L. Zhu, W. Wu, M. Q. Zhu, J. J. Han, J. K. Hurst and A. D. Li, *J. Am. Chem. Soc.*, 2007, **129**, 3524–3526.
55 B. Kim, K. T. Lee, J. Cho, N. A. Darshanoju, K. Jung, I. H. Ahn, J. M. Shin, H. Oh, Y. Ki, H. Lee, S. J. Kwon, I. S. Kim, W. Cai, K. H. Ahn and D. H. Ko, *Adv. Opt. Mater.*, 2021, **9**, 2100776.
56 Y. Xie, M. C. Arno, J. T. Husband, M. Torrent-Sucarrat and R. K. O'Reilly, *Nat. Commun.*, 2020, **11**, 2460.
57 L. Hou, R. Ringstrom, A. B. Maurer, M. Abrahamsson, J. Andreasson and B. Albinsson, *J. Am. Chem. Soc.*, 2022, **144**, 17758–17762.
58 Y.-J. Ma, X. Fang, G. Xiao and D. Yan, *Angew. Chem., Int. Ed.*, 2021, **61**, e202114100.
59 C. Guo, J. Zhai, Y. Wang, X. Du, Z. Wang and X. Xie, *Anal. Chem.*, 2022, **94**, 1531–1536.

60 A. Mokhtar, R. Morinaga, Y. Akaishi, M. Shimoyoshi, S. Kim, S. Kurihara, T. Kida and T. Fukaminato, *ACS Mater. Lett.*, 2020, **2**, 727–735.
61 R. Klajn, *Chem. Soc. Rev.*, 2014, **43**, 148–184.
62 A. A. Ali, R. Kharbash and Y. Kim, *Anal. Chim. Acta*, 2020, **1110**, 199–223.
63 C. Li, A. Iscen, L. C. Palmer, G. C. Schatz and S. I. Stupp, *J. Am. Chem. Soc.*, 2020, **142**, 8447–8453.
64 Y. Liu, M. Fan, S. Zhang, X. Sheng and J. Yao, *New J. Chem.*, 2007, **31**, 1878–1881.
65 S. Cao, L. C. da Silva and K. Landfester, *Angew. Chem., Int. Ed.*, 2022, **61**, e202205266.
66 X. M. Chen, W. J. Feng, H. K. Bisoyi, S. Zhang, X. Chen, H. Yang and Q. Li, *Nat. Commun.*, 2022, **13**, 3216.
67 Z. Chu and R. Klajn, *Nano Lett.*, 2019, **19**, 7106–7111.
68 J. Chen, W. Liu, X. Fang, Q. Qiao and Z. Xu, *Chin. Chem. Lett.*, 2022, **33**, 5042–5046.
69 M.-X. Liu, N. Ding, S. Chen, Y.-L. Yu and J.-H. Wang, *Anal. Chem.*, 2021, **93**, 5284–5290.
70 D. Jin, P. Xi, B. Wang, L. Zhang, J. Enderlein and A. M. van Oijen, *Nat. Methods*, 2018, **15**, 415–423.
71 D. M. Chudakov, V. V. Verkhusha, D. B. Staroverov, E. A. Souslova, S. Lukyanov and K. A. Lukyanov, *Nat. Biotechnol.*, 2004, **22**, 1435–1439.